Journal of Molecular Structure 1232 (2021) 130046

Contents lists available at ScienceDirect

Journal of Molecular Structure

journal homepage: www.elsevier.com/locate/molstr

Directing cation-cation interactions in thiamine compounds: Analysis of a series of organic salts based on vitamin B1

Joseph Traver[a], Erica Chenard[a], Matthias Zeller[b], Gary L. Guillet[c], Will E. Lynch[c], Patrick C. Hillesheim[a,*]

[a] Department of Chemistry and Physics, Ave Maria University, 5050 Ave Maria Blvd, Ave Maria, FL 34142, USA
[b] Department of Chemistry Purdue University, 560 Oval Drive, West Lafayette, IN 47907-2084, USA
[c] Department of Chemistry and Biochemistry, Georgia Southern University, 11935 Abercorn St., Savannah, GA 31419, USA.

ARTICLE INFO

Article history:
Received 27 October 2020
Revised 29 January 2021
Accepted 30 January 2021
Available online 3 February 2021

Keywords:
Crystal structure
Ionic liquids
Hirshfeld surface analysis
Structure-property relationship
Theoretical calculations

ABSTRACT

A series of ionic compounds based on the dicationic vitamin B1 structure have been synthesized and characterized. A set of perfluoroalkyl-based anions, each with a distinct structure, were paired with the cations and the solid-state structures of the salts were analyzed via single-crystal X-ray diffraction. Phase transitions and thermal stability of the compounds were examined via dynamic scanning calorimetry and thermogravimetric analysis. It was found that the salt of the cyclical anion, 1,3-disulfonylhexafluoropropyleneimide $[NCyF]^-$, exhibited higher thermal stability while displaying comparable phase transition temperatures as compared to the linear anionic congeners. The cations within the $[NCyF]^-$ compound were found to interact as paired dimers, a form which is not observed in the other ionic species. Hirshfeld surface analyses supplemented with computational studies of the compounds is used to rationalize and evaluate the distinct properties of the compounds arising from changes in anion geometry.

1. Introduction

The medical and health benefits of vitamin B1 [VB1] (or thiamine/thiamin) have been well documented in the literature. It is considered an essential vitamin and has been the subject of decades, and perhaps centuries, of research [1]. Thiamine, and its related phosphorylated structures, play an active role in various enzymatic pathways and catalytic cycles which have been detailed and summarized through various reviews [1–4].

Of particular importance in biological pathways is the structure of the substrates involved in the cycles. For instance, thiamine has been shown to exhibit various unique conformations in the solid-state referred to as *F*, *S*, or *V* configurations [5]. The distinctions between the configurations are defined by ranges of torsion angles which, in turn, define the plane-angles of the thiazolium and pyrimidinium rings in the cation. Substitutions at the C2 carbon, the presence of phosphate groups at the O53 position (see Fig. 1), and anion geometry have been shown to affect the preference for a specific conformation of the cation [5,6]. The three different conformations of thiamine produce different pockets wherein anions interact forming bridges between the thiazolium and pyrimidinium ring [7,8]. These three pockets are referred to as anion-holes and are aptly named anion-hole I, II, and III. The anion-holes are theorized to play a role in the host-guest properties of the cationic moiety which, in turn, influences the enzymatic processes involving thiamine as well as influence the structural properties of the ionic complex as a whole [1,9–11].

Aside from its purely biological value, the host-guest properties of thiamine have been applied to catalysis. Recently, Tian *et al.* used a derivative of thiamine, in addition to several other thiazolium-based compounds, as catalysts for polymerization reactions [12]. Within their work, interactions between alcohols and carbonyl functional groups on monomers were theorized to interact with specific portions of the thiazolium ring, specifically the π cloud and the C2—H positions on the cationic ring, aiding in the overall performance of their catalytic system. These interactions, both with the π clouds of thiazolium rings [13,14] as well as the C2—H position[15], are well established as relevant points of interactions. Applying a thorough understanding of anion geometry, charge polarization, and atomic composition can lead to the formation of task-specific thiamine-based ionic compounds [16].

The most encompassing definition of the term ionic liquid (IL), is “A liquid comprised entirely of ions” [17]. One of the earliest reports of air and moisture stable ILs came from Wilkes and Za-

* Corresponding author.
E-mail address: patrick.hillesheim@avemaria.edu (P.C. Hillesheim).

https://doi.org/10.1016/j.molstruc.2021.130046
0022-2860/

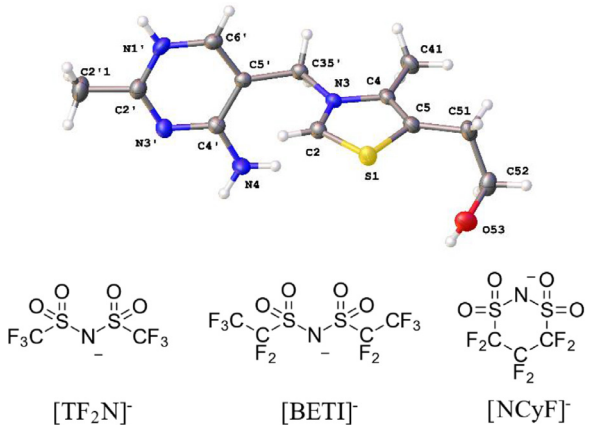

Fig. 1. (top) Dication from **1** depicting the labelling scheme used herein, based on previously reported structures. [6] (bottom) Structures and abbreviations of the anions for compounds discussed herein.

worotoko with their synthesis and characterization of 1-ethyl-3-methylimidazolium tetrafluoroborate or [Emim][BF_4] [18]. This was followed by Fuller *et al.* with their report of using the hexafluorophosphate anion to produce [Emim][PF_6] [19]. To date, both the $[BF_4]^-$ and $[PF_6]^-$ anions remain as some of the most studied anions for the production of ILs [20]. Another popular set of anions for ILs is bis(trifluoromethane)sulfonimide ($[TF_2N]^-$) and bis(pentafluoroethanesulfonyl)imide ($[BETI]^-$) [20,21]. These anions contain perfluoroalkyl chains which, along with the sulfonyl groups, help to disperse the negative charge of the anionic nitrogen. Both $[TF_2N]^-$ and $[BETI]^-$ ILs have demonstrated favorable properties compared to $[PF_6]^-$ and $[BF_4]^-$ based ILs, including lower viscosity, higher thermal stabilities, and increased hydrophobicity, albeit at increased costs of raw materials [22–24].

The related perfluoroalkyl anion 1,3-disulfonylhexafluoropropyleneimide, $[NCyF]^-$, has not seen as much application in the field of ILs when compared to $[TF_2N]^-$ or even $[BETI]^-$. However, a recent study by Kakinuma *et al.* has demonstrated potentially favorable properties of $[NCyF]^-$ desirable for applications of task-specific ILs [25]. For instance, an IL containing the $[NCyF]^-$ anion was used to create fluorescent ILs [26]. Further, the $[NCyF]^-$ was also applied in the development of solid-state conductive materials [27].

Herein we present the synthesis and analysis series of a series of compounds containing the $[TF_2N]^-$, $[BETI]^-$, and $[NCyF]^-$ anions paired with the dicationic thiamine moiety. The thiamine cation presents several unique advantages when compared with traditional imidazolium-based dicationic ILs. For example, thiamine is a task-Further, the synthesis of the ionic compounds presented herein is scalable and simplified to a single metathesis step, bypassing the standard alkylation reaction required for imidazolium ILs. Finally, thiamine is a generally recognized as safe (GRAS) compound [28] potentially negating any toxicity or environmental issues associated with imidazolium-IL systems [29].

There is an active need for the development, characterization, and evaluation of anions for ionic liquid applications [30]. Understanding the structure and interactions of the $[NCyF]^-$ anion, as well as the impacts of the structurally unique $[BETI]^-$ anion, and comparing them with the more established $[TF_2N]^-$ anion will help with the development of tailored IL systems incorporating either the $[BETI]^-$ or $[NCyF]^-$ anions. To evaluate the structural impact of the anions, Hirshfeld surface analysis was performed on both the cationic and anionic portions of all structures. Hirshfeld surface analysis, in brief, examines intermolecular interactions in the crystalline state using a "whole molecule approach" [31,32]. These interactions can then be deconstructed into 2D plots, referred to as fingerprints, allowing for facile comparison of interactions and structural features in multiple samples by simplified visual inspection. [33] To date the work presented herein represents the first Hirshfeld analysis of the thiamineHCl-based dication. Thermogravimetric analysis (TGA) and dynamic scanning calorimetry (DSC) was also performed on the compounds to examine the thermal properties of the salts and evaluate any impact from the changes in anion geometry.

2. Experimental

Thiamine•HCl and lithium bis(trifluoromethane)sulfonimide were purchased from ChemImpex. Lithium 1,3-disulfonylhexafluoropropyleneimide was purchased from TCI Chemicals. Lithium bis(pentafluoroethanesulfonyl)imide was generously donated by Prof. Arsalan Mirjafari at Florida Gulf Coast University. Solvents were purchased from Fisher Scientific. All chemicals were purchased in the highest purity available and used without further purification.

2.1. Computational Studies

All computations and resultant data were obtained using the Spartan software suite (Spartan'18, Wavefunction, Inc., Irvine, CA USA). Initial geometries from the crystal structures of the anions were loaded into the software and optimized employing the ωB97X-D functional[34] with a 6-311++G(d,p) basis set. Vibrational frequencies were checked for imaginary values to ensure the resultant structures were at a minimum.

2.2. Spectroscopy

^1H, ^{13}C, and ^{19}F NMR spectroscopy was performed on a JEOL 400 MHz NMR spectrometer. Acetone-d_6 and Methanol-d_4 were purchased from Cambridge Isotope Laboratories.

2.3. Crystallographic Information

Single crystals of compounds **1** and **2** were coated with a trace of Fomblin oil and were transferred to the goniometer head of a Bruker Quest diffractometer with kappa geometry, a Cu Kα wavelength (λ = 1.54178 Å) I-μ-S microsource X-ray tube, laterally graded multilayer (Goebel) mirror single crystal for monochromatization and a Photon II area detector. A single crystal of **3** was analyzed using a Bruker Quest diffractometer with a fixed chi angle, a sealed tube fine focus X-ray tube, single crystal curved graphite incident beam monochromator, a Photon100 area detector. Both instruments were equipped with Oxford Cryosystems low temperature devices and examination and data collection were performed at 150 K. Data were collected, reflections were indexed and processed, and the files scaled and corrected for absorption using APEX3[35] and SADABS [36]. For all structures, the space groups were assigned and the structures were solved by direct methods using XPREP within the SHELXTL[37] suite of programs and refined by full matrix least squares against F^2 with all reflections using Shelxl2018[38] employing the graphical interface Shelxle [39]. H atoms were positioned geometrically and constrained to ride on their parent atoms. C-H bond distances were constrained to 0.95 Å for aromatic and alkene C-H moieties, and to 0.99 and 0.98 Å for aliphatic CH_2 and CH_3 moieties, respectively. N-H bond distances were constrained to 0.88 Å for planar (sp2 hybridized) NH_2 groups. Alcohol O-H bond distances were constrained to 0.84 Å. Methyl and alcohol H atoms were allowed to rotate, but not to tip, to best fit the experimental electron density. U_{iso}(H) values were set to a

multiple of U_{eq}(C) with 1.5 for CH_3 and 1.2 for C-H and CH_2 units, respectively.

In compound **2**, both anions were refined as disordered. All disordered moieties were restrained to have similar geometries. Methylethylketone and ether solvate molecules are disordered with each other, with oxygen atoms being in similar positions (and H-bound to an N-H group). CH_2-CH_3 distances were restrained to be similar to each other in both solvate molecules. U^{ij} components of ADPs for disordered atoms closer to each other than 2.0 Å were restrained to be similar. Subject to these conditions the occupancy ratio refined to 0.627(4) to 0.373(4) for the anion of S2A/S3A, to 0.9433(14) to 0.0567(14) for the anion of S2B/S3B, and to 0.533(6) to 0.467(6) for the MEK/ether disorder. In compound **3**, anions are extensively disordered. One ion is located in a general position and was refined as disordered over two alternative orientations. Indications for additional disorder are present for this site, but due to the low prevalence (largest Q peak = 0.66 e/Å^3) this additional disorder was ignored. The other two anion sites are located on inversion centers, inducing 1:1 disorder as the ions are incompatible with inversion symmetry. Additional disorder needed to be included to properly fit the observed electron density, and both sites were thus refined as four disordered moieties of which each two were symmetry equivalent. All disordered anion moieties were restrained to have similar geometries. U^{ij} components of ADPs for disordered atoms closer to each other than 2.0 Å were restrained to be similar. Subject to these conditions the occupancy rates refined to 0.696(2) for the anion in the general position, and to two times 0.125(2) and 0.375(2) and two times 0.220(2) and 0.280(2) for the sites with inversion symmetry.

Olex2 was used for structural analysis of the compounds and producing images [40].

CrystalExplorer17 was used for the calculation of the Hirshfeld surfaces and fingerprintplots [41].

Complete crystallographic data, in CIF format, have been deposited with the Cambridge Crystallographic Data Centre. CCDC 2039424, 2039425, and 2039426 contains the supplementary crystallographic data for this paper. These data can be obtained free of charge from The Cambridge Crystallographic Data Centre via www.ccdc.cam.ac.uk/data_request/cif.

It should be noted that when discussing interactions within the crystal structures the D•••A notation is used wherein D and A are the donor and acceptor moieties respectively. The | symbol is used to indicate reciprocal sets of interactions such as D•••A|A•••D.

2.4. Thermal Properties

Phase transitions were measured using a TA instruments Q250 differential scanning calorimeter. Each sample was placed in an aluminum pan and cycled 3 consecutive times from -50°C to 175°C at a heating rate of 10 °C/min and a cooling rate of 10 °C/min. Compound **2** was heated to the same max/min temperatures, but at a rate of 2 °C/min. Temperatures for the phase transitions were determined using the *TRIOS* software from TA Instruments.

Decomposition temperatures were measured on a TA instruments Q500 thermogravimetric analyzer (TGA) using the default dynamic setting for the system and using a platinum pan. Onset decomposition temperatures were taken from the first major weight loss step as calculated using the *TRIOS* software from TA Instruments.

Thermal data were plotted and formatted using the *OriginPro* software suite.

Elemental analyses (C, H and N) were performed by ThermoScientific FLASH 2000 CHNS elemental analyzer. Analytical calculation and the obtained data of all the complexes are presented in the experimental portion as C, H, N percentages. All the calculated data are consistent with the experimental data which are in agreement with the general formula obtained from the single-crystal X-ray analysis excluding any solvent found in the lattice.

2.5. Synthetic procedure

2.5.1. Synthesis of Compound 1, [VB1][TF_2N]$_2$

Thiamine hydrochloride (0.5g, 1 equiv.) and lithium bis(trifluoromethane)sulfonimide (1.0 grams, 2.3 equiv.) were dissolved into a minimal amount of water at room temperature and stirred overnight. The white precipitate that formed was filtered and washed repeatedly with cold water. The white solid was dried under vacuum for three days and used as is without further purification. Yield: 1.1g (89%). Single crystals suitable for diffraction were grown from slow diffusion of hexane into a solution of the compound dissolved in ethyl acetate.

^{1}H NMR (400 MHz; Acetone-d_6) δ 9.92 (s, 1H), 8.64 (s, 1H), 5.94 (s, 2H), 4.51 (t, J = 4.7 Hz, 1H), 3.89 (q, J = 5.3 Hz, 2H), 3.25 (t, J = 5.5 Hz, 2H), 2.74 (d, J = 4.4 Hz, 6H).

^{13}C NMR (101 MHz; Methanol-d_4) δ 165.40 (s, 1C), 164.35 (s, 1C), 147.82 (s, 1C), 143.98 (s, 1C), 138.27 (s, 1C), 125.94 (s, 1C), 122.75 (s, 1C), 119.56 (s, 1C), 116.37 (s, 1C), 106.25 (s, 1C), 61.20 (s, 1C), 51.55 (s, 1C), 30.73 (s, 1C), 21.80 (s, 1C), 11.86 (s, 1C).

^{19}F NMR (376 MHz; Acetone-d_6) δ -79.82 (s, 6F).

Anal. Calcd for $C_{16}H_{18}F_{12}N_6O_9S_5$: C, 23.25; H, 2.19; N, 10.17. Found: C, 23.72; H, 1.76; N, 9.48.

2.5.2. Synthesis of Compound 2, [VB1][NCyF]$_2$

Compound **2** was synthesized following the same procedure as for compound **1** with the substitution of Li[NCyF] in place of Li[TF_2N]. Yield: 1.1g. (90%). Single crystals suitable for diffraction were grown from slow diffusion of diethyl ether into a solution of the compound dissolved in 2-butanone.

^{1}H NMR (400 MHz; Acetone-d_6) δ 9.87 (s, 1H), 8.61 (s, 1H), 5.90 (s, 2H), 4.49 (s, 1H), 3.89 (s, 2H), 3.24 (t, J = 5.5 Hz, 2H), 2.73 (d, J = 2.3 Hz, 6H).

^{13}C NMR (101 MHz; Acetone-d_6) δ 165.13 (s, 1C), 163.97 (s, 1C), 155.70 (s, 1C), 147.86 (s, 1C), 143.56 (s, 1C), 137.87 (s, 1C), 116.82 (m, J = 24.9 Hz, 1C), 113.86 (m, J = 25.1 Hz, 1C), 111.15—110.51 (m, 1C), 108.05 (m, J = 25.7 Hz, 1C), 106.67 (s, 1C), 60.86 (s, 1C), 51.33 (s, 1C), 22.14 (s, 1C), 12.09 (s, 1C).

^{19}F NMR (376 MHz; Acetone-d_6) δ -120.51 (s, 4F), -126.89 (s, 2F)

Anal. Calcd for $C_{18}H_{18}F_{12}N_6O_9S_5$: C, 25.42; H, 2.13; N, 9.88. Found: C, 25.79; H, 1.98; N, 9.72.

2.5.3. Synthesis of Compound 3, [VB1][BETI]$_2$

Compound **3** was synthesized following the same procedure as for compound **1** with the substitution of Li[BETI] in place of Li[TF_2N]. Yield: 0.5g (83%). Single crystals suitable for diffraction were grown from slow diffusion of hexane into a solution of the compound dissolved in isopropyl alcohol.

^{1}H NMR (400 MHz; Acetone-d_6) δ 9.92 (s, 1H), 8.64 (s, 1H), 5.93 (s, 2H), 4.51 (t, J = 4.5 Hz, 1H), 3.89 (q, J = 5.1 Hz, 2H), 3.24 (t, J = 5.5 Hz, 2H), 2.73 (d, J = 4.6 Hz, 6H).

^{13}C NMR (101 MHz; Acetone-d_6) δ 165.17 (s, 1C), 164.02 (s, 1C), 155.74 (s, 1C), 147.76 (s, 1C), 143.63 (s, 1C), 137.93 (s, 1C), 123.50 (s, 1C), 120.64 (t, J = 33.7 Hz, 1C), 117.79 (t, J = 33.7 Hz, 1C), 114.93 (s, 1C), 112.58 (q, J = 38.1 Hz, 1C), 109.67 (d, J = 38.0 Hz, 1C), 106.78 (s, 1C), 60.87 (s, 1C), 51.34 (s, 1C), 22.11 (s, 1C), 12.04 (s, 1C).

^{19}F NMR (376 MHz; Acetone-d_6) δ -79.74 (s, 3F), -118.14 (s, 2F).

Anal. Calcd for $C_{20}H_{18}F_{20}N_6O_9S_5$: C, 23.40; H, 1.77; N, 8.19. Found: C, 23.85; H, 1.69; N, 7.86.

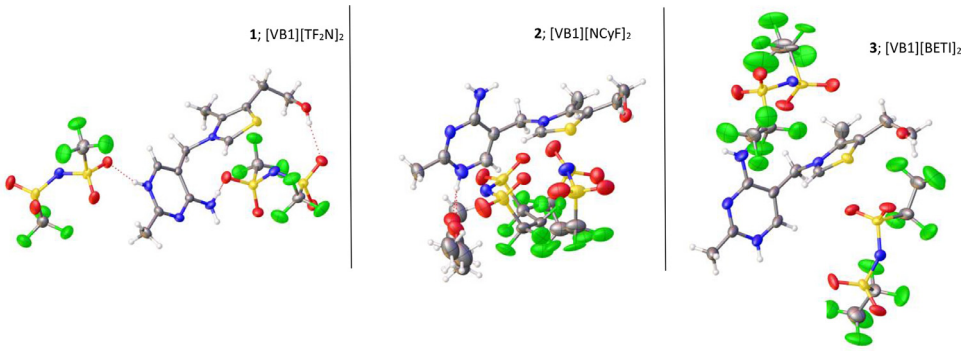

Fig. 2. Asymmetric units for the three structures examined herein shown at 50% probability ellipsoids. Disorder omitted for clarity. Gray - carbon; blue - nitrogen; red – oxygen; yellow - sulfur; green – fluorine.

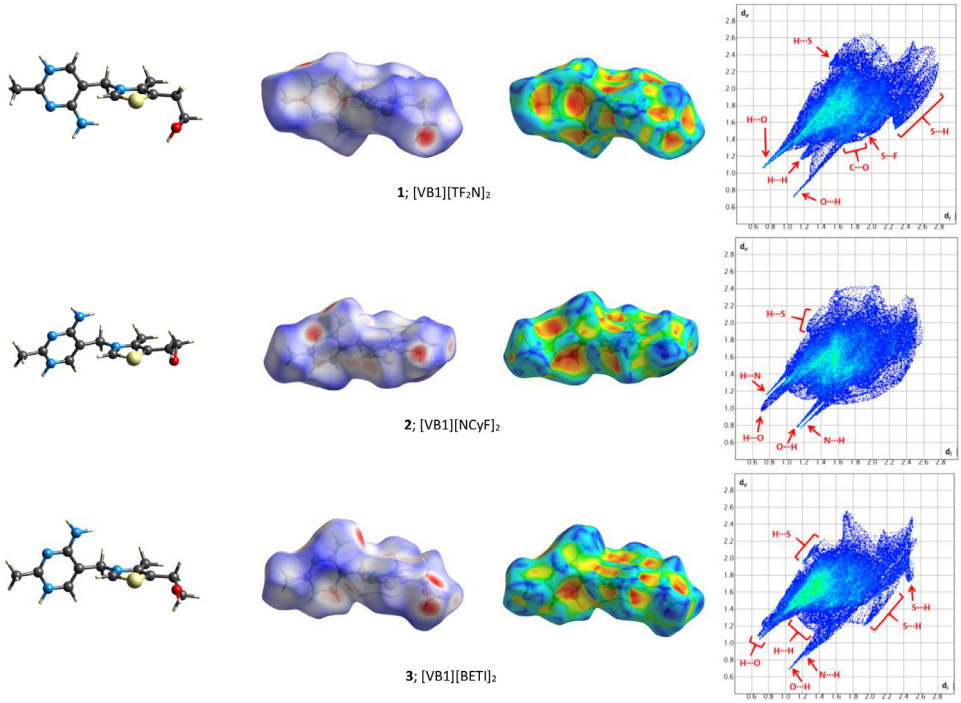

Fig. 3. (Left to right) Cation for reference. Hirshfeld surface mapped with d_{norm}; Hirshfeld surface mapped with the shape index; Fingerprint of the cation.

3. Results and Discussion

3.1. General Cation Discussion

The three crystal structures collected from the compounds are shown in Fig. 2 and the fingerprint plots and surfaces are shown in Fig. 3. Examining the fingerprint plots, several salient features are evident for all the cations. For instance, the fingerprint plots of all the cations exhibit sharp spikes protruding at $d_i \approx 1.1$, $d_e \approx 0.7$ as well as the reciprocal distances. These spikes correspond to hydrogen bonding interactions and are typical features of fingerprint plots [33]. Further, the plots all have an area of high interactions indicated by the green regions in the middle of the blue shape. However, it can be seen that the interactions comprising these green areas are different for each cation, with compound **3** having more interactions in this range indicated by the brighter green color relative to the other cations. The interactions in this green-shaded region correspond predominantly to longer O···H|H···O and N···H|H···N interactions.

Considering hydrogen bond interactions, the cation from **1** is unique among the perfluoroalkane structures in that only two spikes are observed whereas the other cations all show four unique spikes corresponding to the reciprocal sets of shorter O···H|H···O and N···H|H···N interactions. For **2**, cation-cation interactions arise from reciprocal bonds between the acidic hydrogen from the alcohol group (O53—H) and the nitrogen on the pyrimidinium ring (N3'). The cations, interacting through those atoms, form a pocketed dimer and give rise to the characteristic four-spiked fingerprint plots. Compound **1**, however, only exhibits cation-cation hydrogen bonding through O53···H—N4'1 (Fig. 4), forming a zigzagged arrangement with no dimer formation as is observed for **2**. Curiously, N3′ in **1** does not show any short interactions at all which is unique among the structures presented herein. Examining the Hirshfeld surface in the region surrounding N3' in compound **1** one can see only blue or white shaded regions indicating long distance interactions (see Fig. 3). In all other structures examined, the N3′ atom is observed participating in hydrogen bonding with another cation. This point of interaction thus seems a point of variability to tune intramolecular interactions.

Compound **3** also displays distinct cation-cation hydrogen bonding interactions. The fingerprint plot depicts four spikes potentially indicating the formation of the dimeric interactions seen

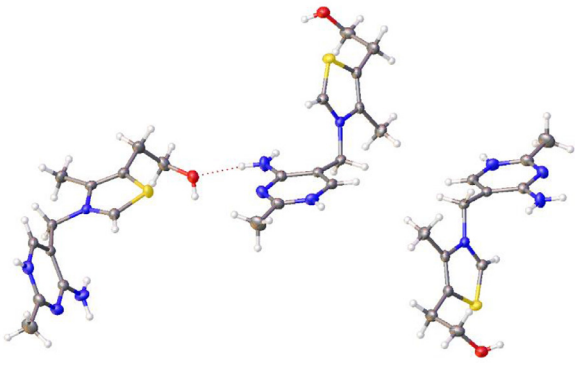

Fig. 4. Cation-cation interactions observed in compound 1 wherein a linear arrangement of cations are linked through N—H•••O hydrogen bonds.

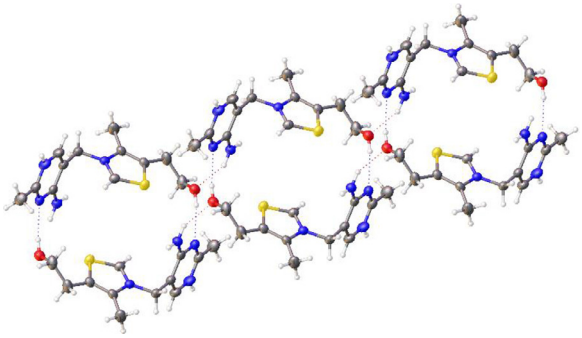

Fig. 5. Cation-cation interactions observed in compound 3 wherein a 'pocket' is formed through the arrangement of the hydrogen bonding.

in **2**; however, the spikes are not as defined. Two of the spikes in **3** are nearly overlapping. The top two prominent spikes both correspond to H···O interactions, with the larger, disperse spike arising from H53 to an adjacent anion. The smaller, pointed spike arises from an N1'—H···O53 interaction between cations and is the shortest of the cation-cation interactions. These N1'—H···O53 interactions link the cations in a manner similar to **1**, with no reciprocal dimeric interactions from the alcohol groups. The bottom N···H spike is from N3'···H—N4'1 interactions with adjacent cations while the reciprocal interaction, that is N4'1—H···N3', is seen as the green region protruding down within the top H···O spike. These interactions represent a cyclical type of hydrogen bonding between the two cations arising from nitrogen functionalities, unique among all the structures examined herein and gives rise, in part, to the unique fingerprint of the cation (see Fig. 5).

While the thiazolium sulfur atom predominantly interacts with O and F atoms, both inter- and intra-molecularly, visually these interactions are often buried within the larger central portions of the fingerprint plots making identification of salient features in the fingerprints for these interactions difficult without examining all of the individually deconstructed plots. One exception is compound **1** wherein S···F interactions form a sharp spike which partially overlaps the C···O π-interactions (see Fig. 3). These S···F interactions are present, however, in nearly all the structures. Given their repeated observation, it is likely these interactions play a role in the packing and formation of the solid-state structures, albeit to a varying degree in each system given the differences observed in the relative percentages of these interactions (see **table S1**). One exception is **2** where the thiazolium sulfur does not exhibit any significant S···F interactions. A negligible amount of interactions are observed with the anion sitting in the anion-hole I pocket, however this accounts for approximately 0.3% of the overall interactions and is far less than in the other structures.

With regards to the H···S interactions, however, all cations display regions of H···S|S···H interactions wherein the sulfur in the thiazolium ring is interacting with a set of adjacent hydrogen atoms located on another cation. Examining the indicated regions on the fingerprint plots reveals characteristic shapes for these interactions, emphasizing the unique structural motifs of the three compounds. For instance, **1** has a defined wing feature arising from S···H interactions, with the shortest interactions to hydrogens on the C2'1 methyl group. Compound **3**, however, shows a spike at shorter distances arising from the same S···H—C2'1 interactions ($d_i \approx 1.9$, $d_e \approx 1.2$). Additionally, **3** has another set of S···H interactions, manifesting as a second spike. These interactions, at $d_i \approx 2.5$, $d_e \approx 1.5$, are between the methylene hydrogens (C52—H) on a symmetry adjacent cation and only observed within compound **3**. It should be noted, however, that these interactions are long-distance and their exact contribution to the overall solid-state structure should be investigated further. However, these salient features in the fingerprint plots are unique and indicative of the distinctive arrangement of the cations within **3**.

Compound **2** displays a series of S···H peaks, manifesting as the spots indicated in the fingerprint plots. The dimeric arrangement of the cations aligns the thiazolium sulfur with hydrogens on C2'1, N4'1, as well as the central thiazolium hydrogen (C2—H) on symmetry adjacent cations. As with a number of these observed S···H interactions, these are all long-distance. However, as has been shown through previous studies, these interactions can have a significant impact on long range arrangement of molecules, especially in biological systems [42–45]. Their recurring presence in all of the structures does lead to the conclusion that they play a role in the formation of the complexes.

Prominent H···H interaction peaks located between the hydrogen bonding spikes are seen in the fingerprint plot of **1**. The shortest interactions arise from C41—H interactions with C6'—H on a symmetry adjacent cation, in addition to other interactions with the ethyl chain hydrogens C51—H and C52—H. The disperse points around the H···H peak, as well as the hydrogen bonding peaks, are indicative of reciprocal hydrogen bonding [33]. Compound **3** also has a region of H···H interaction which is notably unique when compared to **1**. The H···H interactions arising from the C35', C41, C51, and C52 moieties are not present in compound **3** wherein it is observed that these hydrogens instead are interacting with the anions. Finally, the H···H interactions in **2** arise from interactions with the solvent moieties rather than another cation, pointing to the potential for using specific solvents to control the degree of cation-cation interaction.

In conclusion, all cations display a set of similar interactions, specifically the presence of classical hydrogen bonding and H···H interactions. However, close inspection of the fingerprint plots for each structure allows for the determination of unique structural motifs. Compound **2** exhibits unique cation-cation interactions leading to the formation of dimeric structures in the solid-state. This motif is not observed in either compound **1** or **3**. These observations lead to the conclusion that differences in the geometry of the anions can facilitate the formation of unique cation-cation arrangements.

4. General Anion Discussion

The fingerprint plots for the anions from compounds **1** and **2** are shown in Fig. 6 and the individual interactions and percent contributions are listed in **table S1**. The $[BETI]^-$ anions are significantly disordered making comparisons drawn from their fingerprints specious and were thus excluded from surface analysis.

Examining the features of the fingerprint plots, there are shared attributes that are present in all the anions. For instance, as discussed with the cations, there are prominent hydrogen bonding

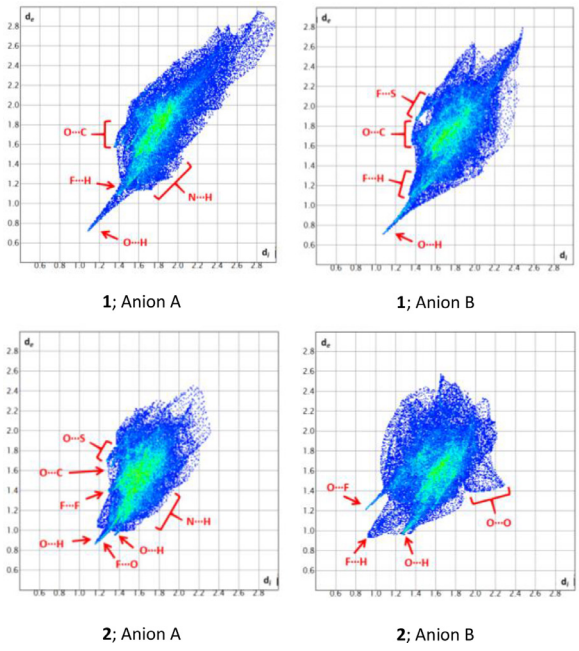

Fig. 6. Fingerprint plots for both anions in the asymmetric units of compounds **1** and **2**.

peaks. The $[TF_2N]^-$ and $[NCyF]^-$ anions, in general, share similar interaction percentages (**table S1**). Further, the relative total percentages of interactions arising from specific atoms share the same trend for both anion sets, wherein the interactions arising from fluorine atoms are most prevalent, followed by interactions from oxygen, and then nitrogen. Curiously, both of the $[TF_2N]^-$ anions exhibit shorter O···H interactions than any of the $[NCyF]^-$ anions. These observations further emphasize that the overall shape of the anions contributes to the unique structural characteristics of the compounds rather than simply atomic composition.

Perhaps the most relevant differences arise from interactions with the central imide nitrogen on the anions. The $[NCyF]^-$ anions show a higher percentage (*ca.* 6%) of interactions arising from the nitrogen while the $[TF_2N]^-$ anions show only an approximate 3.5%. Logically, the $[NCyF]^-$ anion would display increased N···X interactions given the local geometry around the nitrogen making the atom more sterically accessible in addition to the reduced degrees of freedom from the cyclical geometry. This conclusion is supported by computational studies showing the nitrogen on $[NCyF]^-$ has an exposed area of 10.38 $Å^2$ while in the $[TF_2N]^-$ anion (in the trans orientation) the nitrogen has an exposed area of 9.41 $Å^2$. One notable deviation in the overall trends of N···X interactions is with the $[NCyF]^-$ anion B in compound **2** which shows the lowest interaction percentage of all anions. This may be due to the presence of disorder within the anion, however, or is perhaps some more complex effect due to the presence of the solvent.

The $[TF_2N]^-$ anions display overall longer interactions, extending out to $d_i \approx d_e \approx 3.0$ Å with anion A. The $[NCyF]^-$ anions, however, show more contracted interactions, with the overall shape of the $[NCyF]^-$ fingerprints appearing more rounded when compared to the extended shape of the $[TF_2N]^-$. This observation correlates with the geometries of the two anions, with the $[TF_2N]^-$ being more linear as opposed to the ring structure of $[NCyF]^-$. This observation, in part, can be explained by the volumes of the Hirshfeld surfaces for the two structures. The $[TF_2N]^-$ anions have an approximate averaged surface volume of 211 $Å^3$ while the $[NCyF]^-$ have an approximate average volume of 207 $Å^3$.

While all the anions exhibit F···F interactions, the $[NCyF]^-$ anions show distinct spikes in the fingerprints from these interactions. The $[TF_2N]^-$ anions, however, have a larger percentage of F···F interactions as compared to the $[NCyF]^-$ anions despite both anions having the same number of fluorine atoms per moiety. This observation leads to the conclusion that the $[TF_2N]^-$ containing structures should possess more fluorous regions [46].

4.1. $[NCyF]^-$ Anion Structural Discussion

The $[NCyF]^-$ anion approximates a typical cyclohexane-type ring in that it has a preference for a chair conformation which is the most commonly observed conformation in the crystal structure herein and those reported previously [27,47]. This observation was verified using the conformation search algorithm within the Spartan'18 software package, indicating that the chair conformation is the lowest energy conformer of the anion.

With regards to the two anions within the asymmetric unit of **2**, anion A is disordered by rotation while anion B exists as a two-part disordered system, with one part showing the expected chair conformation while the minor moiety is in a twist-boat conformation. This twist-boat conformation is interacting with the adjacent solvent molecule through C—F···H hydrogen interactions, these interactions likely helping to stabilize this conformation of the anion through increased favorable interactions [48]. These interactions, in part, account for anion B having the highest total percentage of F···H interactions of all anions examined.

To better understand the $[NCyF]^-$ anion, all three of the anions were modelled computationally and their calculated structures contrasted to better evaluate similarities and differences. In general, the optimized structures are in good agreement with the molecular structures from the crystals. The optimized structure shows a S2A—N5A distance of 1.601 Å while the crystal structure had a distance of 1.582(3) Å. The concomitant distance, that is S3A—N5A, is 1.576(3) Å. The S—O bond distances were also in good agreement between the crystal and calculated structures with distances of approximately 1.43 Å from the crystals and 1.449 Å calculated. The N—S—N bond angle was observed to be 119.43(16)° and calculated at 121.73°, indicating that the calculated structure is a good model for future studies involving the $[NCyF]^-$ anion.

The electrostatic potential maps for all three anions were calculated to examine the similarities in local atomic charges (see Fig. 7). As expected, the most negative regions are around the oxygen and nitrogen atoms. Looking specifically at the $[NCyF]^-$ anion, the axial oxygen atoms have charges slightly more negative (-0.921 kJ mol^{-1}) than the equatorial oxygen atoms (-0.924 kJ mol^{-1}) which is visualized in the coloring around the oxygen atoms in the electrostatic potential map. The central nitrogen has the most negative charge at -1.209 kJ mol^{-1}. A cavity of positive density (light blue shading) is seen within the ring due to the carbon atoms which range in charge from 0.495 kJ mol^{-1} to 0.628 kJ mol^{-1}. Examining the ESP maps for all three anions, it is clear to see the similarities between the anions, with the negative regions surrounding the oxygen atoms, and the positive areas surrounding the carbons. Natural atomic orbital (NAO) analysis [49] of the atoms complements the visualized potential map.

The highest occupied molecular orbitals (HOMO) for each anion are also shown in Fig. 5. All three anions have similar HOMOs, with the orbitals principally around the oxygen and nitrogen atoms. This explains the interactions between the cations and anions predominantly arising from the O atoms, as has been investigated previously [50]. The calculated orbital energy for the HOMO of $[NCyF]^-$ was found to be -6.4eV, while $[TF_2N]^-$ and $[BETI]^-$ were -6.4eV and -6.6eV respectively.

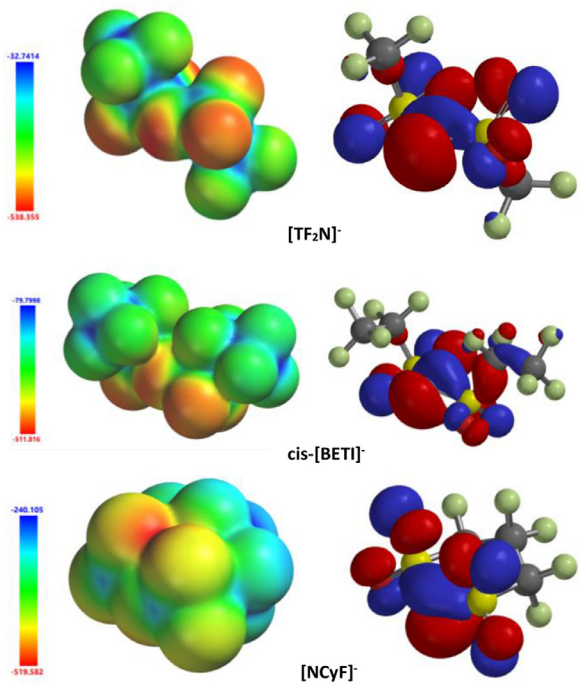

Fig. 7. (left) Electrostatic potential maps of the anions; (right) Highest occupied molecular orbitals.

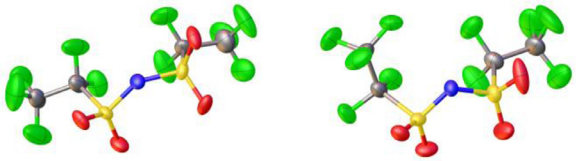

Fig. 8. Two orientations depicting the rotation of the ethyl chain in the cis isomer of $[BETI]^-$.

4.2. $[BETI]^-$ Anion Structural Discussion

Compound **3** is one of the few reported structures [51] containing a $[BETI]^-$ anion reported to date and the first showing the *cis* orientation of the anion making this compound an excellent example to study the solid-state structure and conformation of the anion. The asymmetric unit contains one complete anion and two halves of a $[BETI]^-$ moiety residing on crystallographic special positions. All three of the anionic portions are disordered to varying degrees. The complete $[BETI]^-$ anion is in the *cis* configuration while the anions on the special positions are in the *trans* configuration. As with the related $[TF_2N]^-$ anion, computational studies on the $[BETI]^-$ anion predict a preference for the *trans* configuration over the *cis*, albeit the calculations show that $[BETI]^-$ has a larger energetic preference for *trans* over *cis* [22].

Within the crystal structure, the *cis* anion exhibits N—S—N angles of 118.7° and 142.4° (average 130.5°) for the two disordered portions. The averaged N—S—N angle is slightly larger than the calculated angle at 125.1° although the smallest of the observed angles herein is below the estimated angles from the computational study [22]. Further, within the *cis* anion there exist two orientations of the perfluoroethyl chains, with one orientation exhibiting a staggered orientation and another a gauche orientation with respect to the S—C bond (Fig. 8). The N—S—C—C torsion angles for the staggered and gauche orientation are 160.8(7)° and 51.1(3)° respectively. The staggered orientation places the CF_2 fluorine atoms

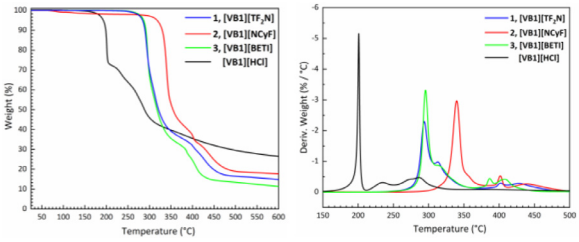

Fig. 9. (left) TGA traces for the compounds the perfluoroalkyl compounds and commercial thiamine HCl as reference; (right) Derivative TGA traces.

within the two chains in close proximity, with an F···F distance of 2.429(12) Å whereas the same CF_2 moieties are further apart in the gauche configuration with an F···F distance of 2.963(6) Å. The gauche conformation, however, does potentially introduce interactions between the CF_2 and CF_3 fluorine atoms on the opposite chain with an observed F···F distance of 3.072(6) Å. No such intramolecular F···F interactions are observed with the *trans* configuration.

4.3. Thermal Properties

The thermal properties of the three perfluoroalkyl salts were examined by TGA and DSC. Examining the TGA plots, a number of similar features are observed (Fig. 9). For instance, all compounds display complex decomposition curves, marked by a large initial decomposition followed by a number of smaller decompositions at higher temperatures ending in a plateau. These smaller, secondary decompositions are best visualized by the derivative TGA curve (dTGA) in Fig. 7. Finally, all compounds produce a noticeable quantity of carbonaceous material during decomposition, with the hydrochloride salt having approximately 30% of its weight remaining at 500°C. This points to the conclusion that the cation is mostly responsible for the decomposition profiles of these compounds given the similarities in the profiles.

Examining the three perfluoalkyl compounds, **1** and **3** display nearly identical traces, with the initial decomposition occurring at approximately 290°C. As expected, this is significantly higher than the hydrochloride decomposition which occurs at approximately 198°C. This observation follows the well-established trend for halide based ionic compounds having lower decomposition temperatures compared with perfluoroalkyl based salts [52]. Examining the dTGA curve from **1** and **3**, their initial decomposition step is marked by a sharp initial step with a shoulder at slightly higher temperatures. This shoulder does not appear as prominent in **2**. Compound **2** has a noticeably higher initial decomposition temperature at 330°C.

DSC traces were also collected for the perfluoro alkyl compounds. As with the TGA data, the phase transitions for the compounds are quite complex with multiple endo and exothermic transitions (see Supplemental Information). While all three compounds display an initial melting transition (Fig. 10), only compound **1** displayed subsequent melting transitions over the three heating and cooling cycles. It is not uncommon, however, for compounds to only show a single melting transition in the timescales of DSC data acquisition [17,53,54]. Compounds **1, 2**, and **3** display comparable melting points of *ca.* 159°C, 164°C, and 164°C respectively. Further, all three compounds exhibit glass transitions on subsequent heating cycles at *ca.* 24°C, 33°C, and 48°C for **1, 2**, and **3** respectively. For reference, commercially sourced [VB1][HCl] shows no phase transitions in the range examined (see Supplemental Information).

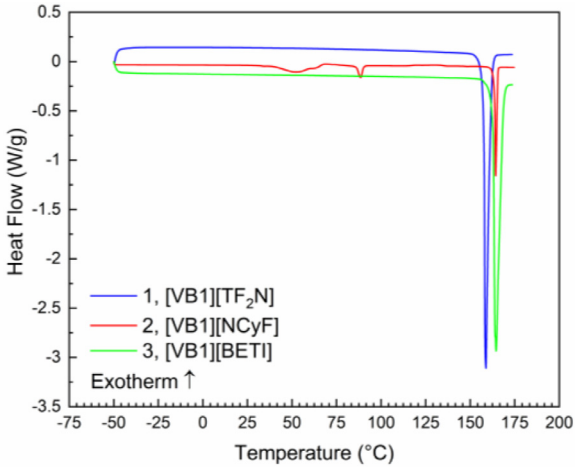

Fig. 10. DSC traces of the 1st heating cycle for the perfluoroalkyl compounds examined.

5. Conclusions

A set of three ionic compounds derived from thiamineHCl paired with perfluoroalkyl anions have been synthesized and their solid-state structures rigorously analyzed by single-crystal X-ray diffraction and Hirshfeld surface analysis. It was found that the cyclical anion, $[NCyF]^-$, produced a structure with comparable melting points but also higher thermal stability as compared to the linear anions $[TF_2N]^-$ and $[BETI]^-$. Preliminary computational studies on the $[NCyF]^-$ anion confirmed a preference for the chair conformation, though an intermediate skew-boat geometry was observed in one of the anions prompting further studies into the geometric preferences for the anion.

The host-guest properties of the thiamine cation seem to be controlled by the structure of the anion present given the noted changes in specific interactions, such as with the pyridinium nitrogen atoms and the arrangement of the cations forming dimeric structures in **2** while linear type interactions are observed with compounds **1** and **3**. Further, **1** crystallizes in the Pbca space group, making it only the third reported thiamine-based orthorhombic structure [55,56].

More rigorous screening for polymorphs and solvated structures is currently underway to help expound the results presented herein. The preliminary data, however, points toward the $[NCyF]^-$ anion as a viable, yet presently expensive, addition to the perfluoroalkyl anion family of compounds commonly employed in the synthesis of ionic liquids.

Declaration of Competing Interest

There are no conflicts to declare.

CRediT authorship contribution statement

Joseph Traver: Methodology, Resources, Investigation. **Erica Chenard:** Methodology, Resources, Investigation. **Matthias Zeller:** Investigation, Writing - review & editing. **Gary L. Guillet:** Data curation, Investigation, Writing - original draft, Writing - review & editing. **Will E. Lynch:** Data curation, Investigation. **Patrick C. Hillesheim:** Conceptualization, Methodology, Validation, Formal analysis, Supervision, Project administration, Writing - original draft, Writing - review & editing.

Acknowledgements

PCH would like to thank the Ave Maria Department of Chemistry and Physics for continued support. The authors would also like to thank Georgia Southern University, Department of Chemistry and Biochemistry for generous use of their X-ray diffractometer in screening of compounds. Parts of this material is based upon work supported by the National Science Foundation through the Major Research Instrumentation Program under Grant No. CHE 1530959, 1919785, and 1625543.

Supplementary materials

Supplementary material associated with this article can be found, in the online version, at doi:10.1016/j.molstruc.2021.130046.

References

[1] S. Manzetti, J. Zhang, D. van der Spoel, Thiamin Function, Metabolism, Uptake, and Transport, Biochemistry 53 (5) (2014) 821–835, doi:10.1021/bi401618y.
[2] M. Louloudi, N. Hadjiliadis, Structural Aspects of Thiamine, Its Derivatives and Their Metal Complexes in Relation to the Enzymatic Action of Thiamine Enzymes, Coord. Chem. Rev. 135–136 (1994) 429–468, doi:10.1016/0010-8545(94)80074-X.
[3] M. Pohl, A New Perspective on Thiamine Catalysis, Curr. Opin. Biotechnol. 15 (4) (2004) 335–342, doi:10.1016/j.copbio.2004.06.002.
[4] S.J. Kashyap, V.K. Garg, P.K. Sharma, N. Kumar, R. Dudhe, J.K. Gupta, Thiazoles: Having Diverse Biological Activities, Med. Chem. Res. 21 (8) (2012) 2123–2132, doi:10.1007/s00044-011-9685-2.
[5] J. Pletcher, M. Sax, G. Blank, M. Wood, Stereochemistry of Intermediates in Thiamine Catalysis. 2. Crystal Structure of DL-2-(.Alpha.-Hydroxybenzyl)Thiamine Chloride Hydrochloride Trihydrate, J. Am. Chem. Soc. 99 (5) (1977) 1396–1403, doi:10.1021/ja00447a019.
[6] N.-H. Hu, T. Norifusa, K. Aoki, Anion Coordination and Molecular Assembly in C2-Substituted Thiamine–Anion Systems: Effects of the Anion and Molecular Conformation, Dalton Trans 3 (2003) 335–341, doi:10.1039/b206765j.
[7] K. Takagi, Y. Hirose, The [Pt1vC1,]2-/Thiamine System. Crystal Structures of (H-Thiamine)[PtCl,] - H,O and (H-Thiamine),[PtCl,]Cl, - 2H20: Host-Guest-like Anion Coordination, Inorg. Chim. Acta 210 (1993) 17–25.
[8] N.-H. Hu, W. Liu, K. Aoki, Thiamine as a Cationic Host in Anion Coordination Chemistry, Bull. Chem. Soc. Jpn. 73 (4) (2000) 1043–1052.
[9] C. Singleton., P Martin, Molecular Mechanisms of Thiamine Utilization, Curr. Mol. Med. 1 (2) (2001) 197–207, doi:10.2174/1566524013363870.
[10] P. Chakravarty, R. Suryanarayanan, Characterization and Structure Analysis of Thiamine Hydrochloride Methanol Solvate, Cryst. Growth Des. 10 (10) (2010) 4414–4420, doi:10.1021/cg100522f.
[11] N.-H. Hu, Y.-S. Liu, K. Aoki, Interactions of Thiamine with Anions: (Hthiamine)(Thiamine) Heptaiododimercurate Dihydrate and Its Dimethanol Monohydrate, Acta Crystallogr. C 55 (3) (1999) 304–308, doi:10.1107/S0108270198013407.
[12] G. Tian, W. Liu, L. Chen, G. Wu, S. Chen, Y. Wang, Thiazolium as Single-Group Bifunctional Catalyst for Selectively Bulk Melt ROP of Cyclic Esters, ChemCatChem 11 (15) (2019) 3388–3392, doi:10.1002/cctc.201900901.
[13] C.R. Kennedy, S. Lin, E.N. Jacobsen, The Cation-π Interaction in Small-Molecule Catalysis, Angew. Chem. Int. Ed. 55 (41) (2016) 12596–12624, doi:10.1002/anie.201600547.
[14] A.S. Mahadevi, G.N. Sastry, Cation–π Interaction: Its Role and Relevance in Chemistry, Biology, and Material Science, Chem. Rev. 113 (3) (2013) 2100–2138, doi:10.1021/cr300222d.
[15] P. Asztalos, C. Parthier, R. Golbik, M. Kleinschmidt, G. Hübner, M.S. Weiss, R. Friedemann, G. Wille, K. Tittmann, Strain and Near Attack Conformers in Enzymic Thiamin Catalysis: X-Ray Crystallographic Snapshots of Bacterial Transketolase in Covalent Complex with Donor Ketoses Xylulose 5-Phosphate and Fructose 6-Phosphate, and in Noncovalent Complex with Acceptor Aldose Ribose 5-Phosphate †, Biochemistry 46 (43) (2007) 12037–12052, doi:10.1021/bi700844m.
[16] H. Davis Jr., J. Task-Specific Ionic Liquids, Chem. Lett. 33 (9) (2004) 1072–1077, doi:10.1246/cl.2004.1072.
[17] Fundamentals of Ionic Liquids, Wiley-VCH Verlag GmbH & Co. KGaA, Weinheim, Germany, 2017, doi:10.1002/9783527340033.
[18] J.S. Wilkes, M.J. Zaworotko, Air and Water Stable I-Ethyl-3-Methylimidazolium Based Ionic Liquids, J. Chemm. Soc. Chem. Commun. (1992) 965–967.
[19] J. Fuller, R.T. Carlin, H.C. De Long, D. Haworth, Structure of 1-Ethyl-3-Methylimidazolium Hexafluorophosphate: Model for Room Temperature Molten Salts, J. Chem. Soc. Chem. Commun. (3) (1994) 299, doi:10.1039/c39940000299.
[20] T. Welton, Ionic Liquids: A Brief History, Biophys. Rev. 10 (3) (2018) 691–706, doi:10.1007/s12551-018-0419-2.
[21] T. Welton, Room-Temperature Ionic Liquids. Solvents for Synthesis and Catalysis, Chem. Rev. 99 (8) (1999) 2071–2084, doi:10.1021/cr980032t.

[22] B. Siu, C.G. Cassity, A. Benchea, T. Hamby, J. Hendrich, K.J. Strickland, A. Wierzbicki, R.E. Sykora, E.A. Salter, R.A. O'Brien, K.N. West, J.H. Davis, Thermally Robust: Triarylsulfonium Ionic Liquids Stable in Air for 90 Days at 300°C, RSC Adv. 7 (13) (2017) 7623–7630, doi:10.1039/C6RA25774G.
[23] J. Dupont, On the Solid, Liquid and Solution Structural Organization of Imidazolium Ionic Liquids, J. Braz. Chem. Soc. 15 (3) (2004) 341–350, doi:10.1590/S0103-50532004000300002.
[24] N.V. Plechkova, K.R. Seddon, Applications of Ionic Liquids in the Chemical Industry, Chem Soc Rev 37 (1) (2008) 123–150, doi:10.1039/B006677J.
[25] S. Kakinuma, T. Ishida, H. Shirota, Femtosecond Raman-Induced Kerr Effect Study of Temperature-Dependent Intermolecular Dynamics in Imidazolium-Based Ionic Liquids: Effects of Anion Species and Cation Alkyl Groups, J. Phys. Chem. B 121 (1) (2017) 250–264, doi:10.1021/acs.jpcb.6b11009.
[26] Q. Zhang, B. Yang, S. Zhang, S. Liu, Y. Deng, Ionic Liquidized-Naphthalenesulfonamide: Successful Fabrication of Liquid Fluorescent Materials, J. Mater. Chem. 21 (41) (2011) 16335, doi:10.1039/c1jm13828f.
[27] M. Moriya, T. Watanabe, S. Nabeno, W. Sakamoto, T. Yogo, Crystal Structure and Solid-State Ionic Conductivity of Cyclic Sulfonylamide Salts with Cyano-Substituted Quaternary Ammonium Cations, Chem. Lett. 43 (1) (2014) 108–110, doi:10.1246/cl.130874.
[28] P.M. Dean, J. Turanjanin, M. Yoshizawa-Fujita, D.R. MacFarlane, J.L. Scott, Exploring an Anti-Crystal Engineering Approach to the Preparation of Pharmaceutically Active Ionic Liquids, Cryst. Growth Des. 9 (2) (2009) 1137–1145, doi:10.1021/cg8009496.
[29] R.J. Bernot, M.A. Brueseke, M.A. Evans-White, G.A. Lamberti, ACUTE AND CHRONIC TOXICITY OF IMIDAZOLIUM-BASED IONIC LIQUIDS ON DAPHNIA MAGNA, Environ. Toxicol. Chem. 24 (1) (2005) 87, doi:10.1897/03-635.1.
[30] A. Benchea, B. Siu, M. Soltani, J.H. McCants, E.A. Salter, A. Wierzbicki, K.N. West, J.H. Davis Jr., An Evaluation of Anion Suitability for Use in Ionic Liquids with Long-Term, High-Temperature Thermal Stability, New J. Chem. 41 (16) (2017) 7844–7848, doi:10.1039/C7NJ01788J.
[31] M.A. Spackman, D. Jayatilaka, Hirshfeld Surface Analysis, CrystEngComm 11 (1) (2009) 19–32, doi:10.1039/B818330A.
[32] M.A. Spackman, J.J. McKinnon, Fingerprinting Intermolecular Interactions in Molecular Crystals, CrystEngComm 4 (66) (2002) 378–392, doi:10.1039/B203191B.
[33] J.J. McKinnon, M.A. Spackman, A.S. Mitchell, Novel Tools for Visualizing and Exploring Intermolecular Interactions in Molecular Crystals, Acta Crystallogr. B 60 (6) (2004) 627–668, doi:10.1107/S0108768104020300.
[34] N. Mardirossian, M. Head-Gordon, ΩB97X-V: A 10-Parameter, Range-Separated Hybrid, Generalized Gradient Approximation Density Functional with Nonlocal Correlation, Designed by a Survival-of-the-Fittest Strategy, Phys. Chem. Chem. Phys. 16 (21) (2014) 9904, doi:10.1039/c3cp54374a.
[35] Apex3 V2019.1-0, SAINT V8.40A, Bruker AXS Inc., Madison (WI), USA, 2019.
[36] L. Krause, R. Herbst-Irmer, G.M. Sheldrick, D. Stalke, Comparison of Silver and Molybdenum Microfocus X-Ray Sources for Single-Crystal Structure Determination, J. Appl. Crystallogr. 48 (1) (2015) 3–10, doi:10.1107/S1600576714022985.
[37] *SHELXTL Suite of Programs, Version 6.14, 2000-2003, Bruker Advanced X-Ray Solutions*; Bruker AXS Inc.: Madison (WI), USA.
[38] G.M. Sheldrick, A Short History of *SHELX*, Acta Crystallogr. A 64 (1) (2008) 112–122, doi:10.1107/S0108767307043930.
[39] C.B. Hübschle, G.M. Sheldrick, B. Dittrich, *ShelXle* : A Qt Graphical User Interface for *SHELXL*, J. Appl. Crystallogr. 44 (6) (2011) 1281–1284, doi:10.1107/S0021889811043202.
[40] O.V. Dolomanov, L.J. Bourhis, R.J. Gildea, J.A.K. Howard, H. Puschmann, *OLEX2* : A Complete Structure Solution, Refinement and Analysis Program, J. Appl. Crystallogr. 42 (2) (2009) 339–341, doi:10.1107/S0021889808042726.
[41] Turner, M. J.; McKinnon, J. J.; Wolff, S. K.; Grimwood, D. J.; Spackman, P. R.; Jayatilaka, D.; Spackman, M. A. *CrystalExplorer17*; University of Western Australia.
[42] L.A.H. van Bergen, M. Alonso, A. Palló, L. Nilsson, F. De Proft, J. Messens, Revisiting Sulfur H-Bonds in Proteins: The Example of Peroxiredoxin AhpE, Sci. Rep. 6 (1) (2016), doi:10.1038/srep30369.
[43] B.R. Beno, K.-S. Yeung, M.D. Bartberger, L.D. Pennington, N.A. Meanwell, A Survey of the Role of Noncovalent Sulfur Interactions in Drug Design, J. Med. Chem. 58 (11) (2015) 4383–4438, doi:10.1021/jm501853m.
[44] B.M. Francuski, S.B. Novaković, G.A. Bogdanović, Electronic Features and Hydrogen Bonding Capacity of the Sulfur Acceptor in Thioureido-Based Compounds. Experimental Charge Density Study of 4-Methyl-3-Thiosemicarbazide, CrystEngComm 13 (10) (2011) 3580, doi:10.1039/c0ce00760a.
[45] P. Zhou, F. Tian, F. Lv, Z. Shang, Geometric Characteristics of Hydrogen Bonds Involving Sulfur Atoms in Proteins, Proteins Struct. Funct. Bioinforma. 76 (1) (2009) 151–163, doi:10.1002/prot.22327.
[46] Canongia Lopes, J.N. A., A.A.H Pádua, Nanostructural Organization in Ionic Liquids, J. Phys. Chem. B 110 (7) (2006) 3330–3335, doi:10.1021/jp056006y.
[47] T. Mochida, Y. Funasako, T. Inagaki, M.-J. Li, K. Asahara, D. Kuwahara, Crystal Structures and Phase-Transition Dynamics of Cobaltocenium Salts with Bis(Perfluoroalkylsulfonyl)Amide Anions: Remarkable Odd-Even Effect of the Fluorocarbon Chains in the Anion, Chem. - Eur. J. 19 (20) (2013) 6257–6264, doi:10.1002/chem.201300186.
[48] K. Reichenbächer, H.I. Süss, J. Hulliger, Fluorine in Crystal Engineering—"the Little Atom That Could, Chem Soc Rev 34 (1) (2005) 22–30, doi:10.1039/B406892K.
[49] F. Weinhold, C.R. Landis, E.D. Glendening, What Is NBO Analysis and How Is It Useful? Int. Rev. Phys. Chem. 35 (3) (2016) 399–440, doi:10.1080/0144235X.2016.1192262.
[50] A. Joseph, V.I. Thomas, G. Żyła, A.S. Padmanabhan, S. Mathew, Theoretical Probing of Weak Anion–Cation Interactions in Certain Pyridinium-Based Ionic Liquid Ion Pairs and the Application of Molecular Electrostatic Potential in Their Ionic Crystal Density Determination: A Comparative Study Using Density Functional Approach, J. Phys. Chem. A 122 (1) (2018) 328–340, doi:10.1021/acs.jpca.7b09189.
[51] D.J. Siegel, G.I. Anderson, N. Cyr, D.S. Lambrecht, M. Zeller, P.C. Hillesheim, A. Mirjafari, Molecular Design Principles of Ionic Liquids with a Sulfonyl Fluoride Moiety, New J. Chem. (2021), doi:10.1039/D0NJ05603K.
[52] S. Zhang (Ed.), Ionic Liquids: Physicochemical Properties, Elsevier, Amsterdam, The Netherlands; Boston; London, 2009.
[53] E. Gómez, N. Calvar, Á. Domínguez, Thermal Behaviour of Pure Ionic Liquids, *Ionic Liquids - Current State of the Art*; Handy, S., Ed.; InTech, 2015, doi:10.5772/59271.
[54] E. Gómez, N. Calvar, Á. Domínguez, E.A. Macedo, Thermal Behavior and Heat Capacities of Pyrrolidinium-Based Ionic Liquids by DSC, Fluid Phase Equilibria 470 (2018) 51–59, doi:10.1016/j.fluid.2018.04.003.
[55] N.H. Hu, S.L. Zhang, Interactions of Thiamine with Anions. Structure of Thiamine Dithiocyanate, Acta Crystallogr. C 49 (6) (1993) 1178–1180, doi:10.1107/S0108270192012630.
[56] W. Shin, M.S. Lah, Structure of Thiamin Naphthalene-1,5-Disulfonate Monohydrate, Acta Crystallogr. C 43 (1) (1987) 125–129, doi:10.1107/S0108270187096768.